Ion broadening of dense-plasma spectral lines including field-dependent atomic physics and the ion quadrupole interaction

D. P. Kilcrease,* R. C. Mancini, and C. F. Hooper, Jr.
Department of Physics, University of Florida, Gainesville, Florida 32611
(Received 24 March 1993; revised manuscript received 7 July 1993)

We examine the theoretical line spectra from hydrogenlike argon in the electron-number-density range of 10^{24}–10^{25} cm^{-3} and at a temperature corresponding to $kT=800$ eV. At these high densities it is important to address the relevance of higher-order plasma-ion microfield effects on the spectral line shape. We begin by calculating spectral line shapes using electric-field-dependent matrix elements that are constructed from wave functions which are solutions of Schrödinger's equation for hydrogenic ions in a uniform field. This provides a suitable basis for including microfield spatial nonuniformities by considering the quadrupole term in the radiator-perturbing ion interaction. Field gradients are calculated in an approximation that takes ion-ion correlations into account. We examine the consequences of these effects as well as of mixing between the adjacent Stark manifold on the Lyman-α and Lyman-β lines of hydrogenlike argon.

PACS number(s): 52.25.Nr, 32.70.Jz, 32.30.Rj

I. INTRODUCTION

For a number of years, x-ray line spectroscopy has been used as a noninvasive diagnostic of hot dense plasmas [1,2]. At the present time this diagnostic technique finds application in the diagnosis of temperature and density in dense plasmas created by inertial confinement and other means. In particular, Stark broadening has been used to infer electron number densities up to $(2-8)\times10^{24}$ cm^{-3} [3]. Since the trend in these experiments is for even higher densities, it is important to examine further the consequences of the concomitant high-strength plasma electric microfields generated in such plasmas. At lower densities, the assumption of a uniform microfield at the radiator is usually made. As the density increases and the interion distances decrease, this assumption becomes questionable due to the existence of significant microfield gradients [4–9]. These field nonuniformities were first treated in detail by the inclusion of the ion quadrupole effect by Demura and Sholin [4]. Also, adjacent Stark manifolds will begin to mix [10,11] and the resonance nature of the atomic states becomes more apparent. For weak fields these resonances are very similar in character to the unperturbed bound states and can be treated by perturbation theory. However, as the plasma field strength becomes comparable to the field produced by the nucleus of the radiating atom or ion, a nonperturbative treatment is needed.

In this paper we will examine some of the consequences of these high-density effects on the Lyman-α and Lyman-β lines of hydrogenic argon. We will focus on the electron-number density range of 10^{24}–10^{25} cm^{-3} at a temperature corresponding to 800 eV. The onset of significant electron degeneracy (not included in our formulation) imposes the upper limit on the density examined in this paper. We choose as the atomic basis set for this problem the set of wave functions that are solutions to Schrödinger's equation corresponding to a hydrogenic ion in a uniform electric field. This exact treatment of the uniform field avoids the usual perturbation theory approach typically used for weaker fields. Using this field-dependent basis we will treat, perturbatively, field nonuniformities by the inclusion of the ion quadrupole term from the multipole expansion of the radiator-perturbing ion interaction.

Our theoretical development follows standard methods which impose the quasistatic ion approximation. Since we examine the spectra of ions in a pure argon plasma, ion dynamics effects will not be significant [12]. The effect of the dynamic perturbing electrons is treated by the Smith-Hooper relaxation theory to second order in the electron-radiator interaction [13,14]. The evaluation of the ion quadrupole term is carried out using a field constrained average employing the adjustable parameter exponential approximation (APEX) model of the plasma-ion microfield [15,16] thus also incorporating correlations among perturbing ions. This represents an improvement with respect to a previous treatment that only included correlations between the radiator and perturbing ions [6].

The power emitted by dipole radiation from an emitter immersed in a plasma, as a function of the frequency, is given by [1,17]

$$P(\omega)=\frac{4\omega^4}{3c^3}I(\omega)\ , \tag{1}$$

where $I(\omega)$, the line-shape function, is defined by

$$I(\omega)\equiv\sum_{a,b}\delta(\omega-\omega_{ab})|\langle b|\mathbf{d}|a\rangle|^2\rho_a\ . \tag{2}$$

Here a and b refer to the initial and final states of the total radiator-plasma system, respectively. The energy difference between these initial and final states is $\omega_{ab}=(E_a-E_b)/\hbar$. The dipole moment of the radiator is given by $\mathbf{d}$ and the population of the initial states is given

by ρ_a, which is an eigenvalue of the density matrix ρ, where $\rho=\sum_i \rho_i |i\rangle\langle i|$. The eigenvectors $|i\rangle$ are eigenfunctions of the system Hamiltonian.

Our system will consist of plasma electrons, ions, and the radiator which will always be referred to by the subscripts e, i, and r, respectively. It is convenient to represent the line-shape function as the transform of a dipole-dipole autocorrelation function $\phi(t)$,

$$I(\omega)=\frac{1}{\pi}\mathrm{Re}\int_0^\infty dt\, e^{i\omega t}\phi(t)\ , \tag{3}$$

where $\phi(t)$ is given by [1]

$$\phi(t)=\mathrm{Tr}_{r,e,i}[\mathbf{d}(0)\cdot\mathbf{d}(t)\rho]\ . \tag{4}$$

Here the subscripts refer to the trace over electron, radiator, and ion coordinates and $\mathbf{d}(t)$ is the radiator dipole operator in the Heisenberg representation.

The multipole expansion [18] of the radiator-perturbing ion interaction is given by

$$V_{r,i}=\chi\varphi(0)-\mathbf{d}\cdot\mathbf{E}(0)-\tfrac{1}{6}\sum_{i,j} Q_{i,j}\frac{\partial E_i(0)}{\partial x_j}+\cdots\ . \tag{5}$$

The electric fields and potentials refer to those produced by the plasma ions at the radiator which we take to be located at the origin. The first three terms are the monopole, the ion dipole, and the ion quadrupole, respectively. The effective charge of the radiator is given by $\chi=Z-\alpha$, where Z is the radiator charge and α is the number of bound radiator electrons. The components of the radiator quadrupole moment tensor are given by $Q_{i,j}$. The octupole term is fourth order in the expansion parameter δ compared to the third-order quadrupole term ($\delta=r_n/r_{o,i}$, where r_n is the electron Bohr orbital radius for a radiator of principal quantum number n and $r_{o,i}$ is the ion sphere radius). For the special case of hydrogenlike ions, it has been shown [19] that the octupole term, to first order in perturbation theory, produces symmetric shifts of the hydrogenic energy levels and thus will not contribute significantly to the asymmetry of the line. The quadrupole term, however, typically induces an asymmetry in the spectral line shape. Since we are using a basis set for this calculation that is made up of eigenfunctions of the radiator Hamiltonian that includes the field-dependent dipole term, we take the quadrupole term as the first-order correction to this Hamiltonian and neglect all higher-order terms.

We symbolically represent all field-gradient terms $\partial E_i(0)/\partial x_j$ or $\partial_i E_j$ by the generic term $E_{\mu\nu}\equiv\partial_\mu E_\nu$. By using the standard technique of introducing a delta function and factoring the density matrix [20], we can express $\phi(t)$ as

$$\phi(t)=\int d\boldsymbol{\epsilon}\int d\epsilon_{\mu\nu}\mathrm{Tr}_{r,e,i}[\rho_i\delta(\boldsymbol{\epsilon}-\mathbf{E})\delta(\epsilon_{\mu\nu}-E_{\mu\nu})\times\mathbf{d}(0)\cdot\mathbf{d}(t)\rho_{r,e}]\ . \tag{6}$$

Here the integration variable $\epsilon_{\mu\nu}$ is used in the same way as $E_{\mu\nu}$ above to represent all relevant partial derivatives. The system ion coordinates have now been separated from the radiator and perturbing electron subsystems. This is expressed by the use of Eq. (6) in Eq. (3) to give

$$I(\omega)=\int d\boldsymbol{\epsilon}\int d\epsilon_{\mu\nu}W(\boldsymbol{\epsilon},\epsilon_{\mu\nu})J(\omega,\boldsymbol{\epsilon},\epsilon_{\mu\nu})\ , \tag{7}$$

where $W(\boldsymbol{\epsilon},\epsilon_{\mu\nu})$ is the ion joint probability function and $J(\omega,\boldsymbol{\epsilon},\epsilon_{\mu\nu})$ is the line-shape function for a radiator in the presence of a uniform field $\boldsymbol{\epsilon}$ and a field gradient represented by $\epsilon_{\mu\nu}$. $W(\boldsymbol{\epsilon},\epsilon_{\mu\nu})$ is given by

$$W(\boldsymbol{\epsilon},\epsilon_{\mu\nu})=\mathrm{Tr}_i[\rho_i\delta(\boldsymbol{\epsilon}-\mathbf{E})\delta(\epsilon_{\mu\nu}-E_{\mu\nu})] \tag{8}$$

and is discussed further in Sec. II. The line-shape function is given by

$$J(\omega,\boldsymbol{\epsilon},\epsilon_{\mu\nu})=\frac{1}{\pi}\mathrm{Re}\,\mathrm{Tr}_{r,e}[\mathbf{d}(0)\cdot\mathbf{d}(t)\rho_{r,e}]\ . \tag{9}$$

The theoretical development of this expression proceeds in the standard way [13,21] with the exception that the zero-order radiator Hamiltonian $H_r(\boldsymbol{\epsilon})$ contains the dipole part of the radiator-ion multipole expansion. The ion quadrupole term that describes the field gradient is treated as the lowest-order correction.

We will consider the first two hydrogenic ion resonance lines: the L_α and L_β. For hydrogenic ions at the density and temperature we will be considering, the ground state is only very weakly affected by the plasma. Therefore we will ignore any lower state broadening and interference effects, and the resulting line-shape function will be given by

$$J(\omega,\boldsymbol{\epsilon},\epsilon_{\mu\nu})=-\frac{1}{\pi}\mathrm{Im}\sum_{a,a'}\rho_a\mathbf{d}_{af}\cdot\mathbf{d}_{fa'}\{\omega-[H_r(\boldsymbol{\epsilon},\epsilon_{\mu\nu})-\omega_f]-M(\omega)\}^{-1}_{aa'}\ , \tag{10}$$

where ω_f is the lower state energy of the radiator; a and a' denote upper states. For simplicity we have set $\hbar=1$. The Hamiltonian $H_r(\boldsymbol{\epsilon},\epsilon_{\mu\nu})$ is given by

$$H_r(\boldsymbol{\epsilon},\epsilon_{\mu\nu})=H_r(\boldsymbol{\epsilon})-\tfrac{1}{6}\sum_{i,j}Q_{i,j}\partial_i\epsilon_j\ , \tag{11}$$

where $H_r(\boldsymbol{\epsilon})$ is the field-dependent Hamiltonian

$$H_r(\boldsymbol{\epsilon})=H_r^0-\mathbf{d}\cdot\boldsymbol{\epsilon}\ , \tag{12}$$

and H_r^0 is the field-free Hamiltonian. The electron broadening operator matraix elements are given approximately by [14]

$$M(\omega)_{aa'}=-\frac{i}{3}\sum_{a''}\mathbf{d}_{aa''}\cdot\mathbf{d}_{a''a'}G(\Delta\omega_{a''f})\ , \tag{13}$$

where the subscript f refers to the single lower radiator state. Here $G(\Delta\omega)$ is the electron many-body function [14,22]. Note that the electron broadening matrix elements $M(\omega)_{aa'}$ are field dependent due to the field dependence of the dipole matrix elements $\mathbf{d}_{a,a'}$ as well as the field dependence of $\Delta\omega_{a''f}$.

II. THE ION-QUADRUPOLE EFFECT

The ion coordinate joint probability function $W(\boldsymbol{\epsilon},\epsilon_{\mu\nu})$ [Eq. (8)] has been introduced to describe the joint probability distribution for the microfield $\boldsymbol{\epsilon}$ and the field gradients $\epsilon_{\mu\nu}$. Writing out this probability function explicitly gives

$$W(\epsilon,\epsilon_{\mu\nu})=\left\langle \delta(\epsilon-\mathbf{E})\prod_{\substack{i,j=1\\ i\geq j}}^{3}\delta(\epsilon_{ij}-E_{ij})\right\rangle_i$$
$$=\frac{1}{Z_c}\int e^{-\beta V}\delta(\epsilon-\mathbf{E})\prod_{\substack{i,j=1\\ i\geq j}}^{3}\delta(\epsilon_{ij}-E_{ij})d^{3N}r\ , \tag{14}$$

where subscripts 1, 2, and 3 represent the spatial indices x, y, and z. Here $\langle\ \rangle_i$ is the ensemble average over ion coordinates, Z_c is the configurational partition function for the ion subsystem, N is the number of ions, and V is the potential energy of the ion subsystem in the presence of the charged radiator. The quantities $\mathbf{E}$ and E_{ij} are the many-particle electric field and field gradients at the radiator and are functions of the perturbing ion coordinates. Use of integral representations for the field-gradient delta functions gives

$$W(\epsilon,\epsilon_{\mu\nu})=\frac{1}{(2\pi)^6}Q(\epsilon)\int d^6\sigma\ \exp\left[-i\sum_{i,j}\sigma_{ij}\epsilon_{ij}\right]\langle e^{i\Theta}\rangle_\epsilon$$
$$=Q(\epsilon)P(\epsilon_{\mu\nu}|\epsilon)\ , \tag{15}$$

where

$$\Theta=\sum_{i,j}\sigma_{ij}E_{ij} \tag{16}$$

and

$$Q(\epsilon)=\frac{1}{Z_c}\int d^{3N}r\,e^{-\beta V}\delta(\epsilon-\mathbf{E})\ . \tag{17}$$

Here $Q(\epsilon)$ should not be confused with the components of the quadrupole tensor $Q_{i,j}$. We have defined the conditional averaged quantity

$$\langle e^{i\Theta}\rangle_\epsilon\equiv\frac{\int d^{3N}r\,e^{-\beta V}\delta(\epsilon-\mathbf{E})e^{i\Theta}}{\int d^{3N}r\,e^{-\beta V}\delta(\epsilon-\mathbf{E})}\ . \tag{18}$$

This is the ensemble average of $e^{i\Theta}$ where all included ion configurations are constrained to give the microfield value ϵ. By defining the average in this way we have retained the benefits of using the ordinary plasma microfield function $Q(\epsilon)$ to describe the probability of the uniform field at the radiator and we are now free to approximate the higher-order field gradients as necessary. The function $P(\epsilon_{\mu\nu}|\epsilon)$ is the conditional probability for the field derivatives $\epsilon_{\mu\nu}$ given ϵ. For simplicity we take the field to be in the z direction.

Direct evaluation of this constrained average is difficult if we wish to retain the full influence of the field gradient. Consequently, we make a simple approximation to this function. We expand the exponential in a cumulant expansion [23] by taking

$$\langle e^{i\Theta}\rangle_\epsilon=\exp\left[\sum_{n=1}^{\infty}\frac{(i)^n}{n!}C_n\right]\ , \tag{19}$$

where the first two coefficients are given by $C_1=\langle\Theta\rangle_\epsilon$ and $C_2=\langle\Theta^2\rangle_\epsilon-\langle\Theta\rangle_\epsilon^2$. If we retain only the C_1 term as an approximation, this gives

$$\langle\epsilon^{i\Theta}\rangle_\epsilon\approx e^{i\langle\Theta\rangle_\epsilon}\ , \tag{20}$$

which is equivalent to replacing the field gradient by its average value. Retention of the C_2 term in the expansion in Eq. (19) leads to corrections to the Hamiltonian that are centered about the average $\langle E_{ii}\rangle_\epsilon$ but are governed by a bivariate normal distribution in the E_{xx} and the E_{zz} terms (the E_{yy} terms can be eliminated). Contributions from the cross terms E_{ij} for $i\neq j$ are governed by normal distributions that are distributed about $\langle E_{ij}\rangle_\epsilon=0$. The variances of these distributions are of third order in the expansion parameter δ. The distribution $P(\epsilon_{\mu\nu}|\epsilon)$ can, in principle, be evaluated explicitly including the C_1 and C_2 terms; here we will explore the effect of including only C_1. The results of including C_2 will be presented in a separate paper.

Substitution of Eq. (20) into Eq. (15) gives

$$P(\epsilon_{\mu\nu}|\epsilon)=\delta(\epsilon_{\mu\nu}-\langle E_{\mu\nu}\rangle_\epsilon)\ . \tag{21}$$

This results in a calculationally simple and useful approximation. Returning to the expression for the spectral line intensity, Eq. (7) with the use of Eq. (15) now gives

$$I(\omega)=\int d\epsilon\int d\epsilon_{\mu\nu}Q(\epsilon)P(\epsilon_{\mu\nu}|\epsilon)J(\omega,\epsilon,\epsilon_{\mu\nu})\ . \tag{22}$$

Since the microfield function $Q(\epsilon)$ depends only on the magnitude of ϵ, we can write

$$P(\epsilon)\equiv 4\pi\epsilon^2Q(\epsilon)\ . \tag{23}$$

Using Eq. (21) for $P(\epsilon_{\mu\nu}|\epsilon)$ we can carry out the $\epsilon_{\mu\nu}$ integrations to obtain

$$I(\omega)=\int d\epsilon\,P(\epsilon)J(\omega,\epsilon,\langle E_{\mu\nu}\rangle_\epsilon)\ . \tag{24}$$

The field-gradient terms in $J(\omega,\epsilon,\epsilon_{\mu\nu})$ have now been replaced with their constrained averages whose only field dependence is ϵ. To evaluate the ion quadrupole term note that the perturbed radiator Hamiltonian [Eq. (11)] is now

$$H_r(\epsilon,\langle E_{\mu\nu}\rangle_\epsilon)=H_r(\epsilon)-\tfrac{1}{6}\sum_{i,j}Q_{i,j}\langle E_{ij}\rangle_\epsilon\ . \tag{25}$$

$\langle E_{ij}\rangle_\epsilon$ may be evaluated by making use of the tracelessness of the quadrupole tensor [18], the property $\partial_jE_i=\partial_iE_j$, the fact that $\langle E_{ij}\rangle_\epsilon=0$ for $i\neq j$, and the equivalence $\langle E_{xx}\rangle_\epsilon=\langle E_{yy}\rangle_\epsilon$ to give the expression

$$\sum_{i,j}Q_{i,j}\langle E_{ij}\rangle_\epsilon=\tfrac{3}{2}Q_{zz}(\langle E_{zz}\rangle_\epsilon-\tfrac{1}{3}\langle\nabla\cdot\mathbf{E}\rangle_\epsilon)\ . \tag{26}$$

If the ion interaction potentials are screened we have $\nabla\cdot\mathbf{E}\neq 0$ due to the continuous charge distribution. However, the form of the multipole expansion we have employed assumes $\nabla\cdot\mathbf{E}=0$ at the radiator, which is not strictly true for the screened ion potentials used in plasma microfield models. We reconcile these two facts by noting that if we restrict the screening charge density of the perturbing ions to lie outside the Bohr orbit of the radiator's bound electron, we will have $\nabla\cdot\mathbf{E}=0$ at the radiator. This gives

$$H_r(\epsilon,\langle E_{\mu\nu}\rangle_\epsilon)=H_r(\epsilon)-\tfrac{1}{4}Q_{zz}\langle E_{zz}\rangle_\epsilon\ . \tag{27}$$

In the Appendix it is shown that $\langle E_{zz} \rangle_\epsilon$ can be related to a functional derivative of the plasma microfield generating functional.

In this work we choose the APEX approximation [15,24–26] for this microfield generating functional. It has the advantage of incorporating correlations between the perturbing ions while retaining the functional simplicity of the independent-perturber (IP) model of the microfield. We will also use an IP model to evaluate the ion quadrupole effect which will lead to an underestimate of its magnitude due to the neglect of the correlations among perturbing ions. We will compare these two models along with a nearest-neighbor (NN) approximation for the field gradient.

The APEX model for the microfield is based on the independent perturber model but with an effective inverse screening length α. The field is effectively renormalized in this way by requiring that two conditions [15] on $Q(\epsilon)$ be met: the so-called second moment condition and the local field condition. The transformed conditional distribution function $\tilde{g}(\mathbf{r};\boldsymbol{\lambda})$ for the APEX microfield distribution is given by [16]

$$\tilde{g}(\mathbf{r};\boldsymbol{\lambda})=\frac{\delta G[\phi]}{\delta(i\boldsymbol{\lambda}\cdot\mathbf{E}(\mathbf{r}))}=n_i g(r) e^{i\boldsymbol{\lambda}\cdot\mathbf{E}^*(\mathbf{r})} , \tag{28}$$

where $g(r)$ is the equilibrium radial distribution function and $\mathbf{E}^*(\mathbf{r})$ is the APEX renormalized field. This field is given by

$$\mathbf{E}^*(\mathbf{r})=Z_i e\frac{\mathbf{r}}{r^3}(1+\alpha r)e^{-\alpha r} , \tag{29}$$

where the parameter α is determined by the above two conditions and Z_i is the perturbing ion charge. The required radial distribution function $g(r)$ is calculated by integral equation methods due to Rogers [27]. Lado and Dufty [16] have shown that this method for evaluating Eq. (28) by using the APEX microfield tends to underestimate the interion correlations. We retain the APEX model, however, because of its simplicity and significant improvement over the IP model of Joyce [6,19]. The evaluation of $\langle E_{zz} \rangle_\epsilon$ is carried out in the Appendix.

We examine the behavior of the field gradient term $\langle E_{zz} \rangle_\epsilon$ in the limit of large and small values of ϵ. For $\epsilon \to 0$ it is easy to show that the field dependence follows the limit of the spherical Bessel function of the first kind $j_2(k\epsilon)$ to lowest order in ϵ. This will give

$$\lim_{\epsilon\to 0} \langle E_{zz} \rangle_\epsilon = -C\epsilon^2 , \tag{30}$$

where C is a constant that depends on n_e, T, and Z_i. Thus the zero-field limit is zero as is expected from symmetry considerations. The large-field behavior of the microfield at a charged radiator is governed by a single nearest-neighbor ion [28]. For the strongest fields, the nearest neighbor will be inside the screening length $\lambda_{D,e}$ so screening will be negligible. To approximate $\langle E_{zz} \rangle_\epsilon$ let the field gradient at the radiator be that produced by a single ion located at the distance from the radiator sufficient to give a field value at the radiator of ϵ. This gives the nearest-neighbor approximation

$$\langle E_{zz} \rangle_{\epsilon,\mathrm{NN}} = -\frac{2}{\sqrt{Z_i}}\left[\frac{e}{r_{o,e}^3}\right]\bar{\epsilon}^{3/2} \tag{31}$$

for large ϵ. Here $\bar{\epsilon}=\epsilon/\epsilon_o$ with $\epsilon_o = e/r_{o,e}^2$, where $r_{o,e}$ is the electron sphere radius.

In Fig. 1 we show the behavior of the APEX model for the field gradient at several values of the electron-number density. For the largest density we see that the magnitude of the field-gradient term begins to approach the nearest-neighbor limiting value as the field increases. The difference between these two models can be attributed to many-body effects. These effects will play a decreasing role for the larger field cases because more than one perturbing ion in close proximity to the radiator is required for many-body effects to be important. The probability of having two perturbing ions located close to the radiator, however, is small [28] because of mutual repulsion leading to the dominance of the nearest-neighbor contribution to the field gradient at large field values. For comparison with the APEX model for the field gradient we introduce an IP model that neglects correlations among perturbing ions but retains the correlations between perturbing ion and the central charged radiator. To accomplish this we use the simple Debye-Hückel approximation to the radial distribution function $g(r)$ [29] with screening provided by electrons only. For a given density the results of the IP model for the magnitude of the field gradient falls below that of the APEX model. This is also illustrated in Fig. 1 for a single density. The net effect of introducing ion-ion correlations into our model is to increase the magnitude of the constrained average field gradient as compared to that calculated from the IP model.

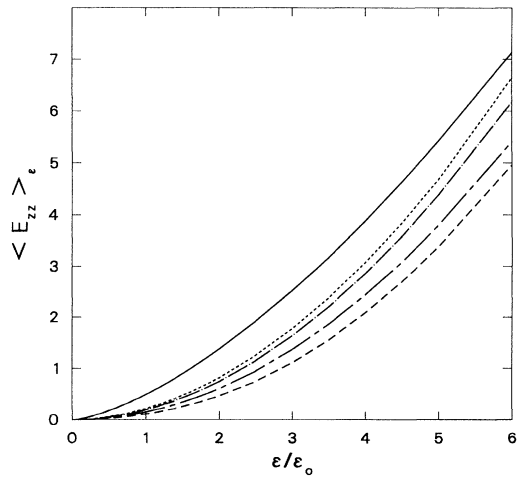

FIG. 1. Comparison of the magnitude of the constrained average field-gradient term $\langle E_{zz} \rangle_\epsilon$ to the nearest-neighbor limiting case for varying density. —·—· refers to $n_e=1\times10^{24}$ cm^{-3}, –·–·–· refers to $n_e=5\times10^{24}$ cm^{-3}, ------ refers to $n_e=1\times10^{25}$ cm^{-3}, and —— refers to the nearest-neighbor model discussed in the text. For comparison the IP (no ion-ion correlations) approximation is given by ——————— for $n_e=1\times10^{24}$ cm^{-3}. All temperatures are $kT=800$ eV and the field gradient is in units of $e/r_{o,e}^3$.

This will result in a corresponding increase in the magnitude of the ion quadrupole effect on the spectral line shape.

III. ATOMIC DATA FOR THE EVALUATION OF MATRIX ELEMENTS

To evaluate the necessary matrix elements for the radiator subsystem for the calculation of the spectral line shape $I(\omega)$, we are free to use any complete set of basis states that spans the Hilbert space of the system. The usual basis set consists of the eigenvectors of the field-free radiator Hamiltonian. We will employ an alternative basis set that consists of the eigenvectors of a radiator Hamiltonian [Eq. (12)] that includes the ion dipole term from the perturbing-ion multipole expansion. This Hamiltonian is diagonal in the field-dependent basis set, and by its use we automatically incorporate the major effects of the perturbing plasma electric microfield into the problem. Specifically, we will use $H_r(\epsilon)$ as our zero-order radiator Hamiltonian. The first-order correction to this will be the next term in the perturbing-ion multipole expansion, the ion quadrupole term. Throughout this paper we use the term "field-dependent atomic physics" to refer to energy values and wave functions (and resulting matrix elements) obtained from the Hamiltonian $H_r(\epsilon)$.

To calculate our field-dependent basis we solve Schrödinger's equation in the position representation with the Hamiltonian $H_r(\epsilon)$,

$$H_r(\epsilon)\psi(\mathbf{r})=E\psi(\mathbf{r}) . \tag{32}$$

The natural coordinates to use for this Hamiltonian are parabolic coordinates [30,31] since the wave equation is then separable and solutions can be sought of the form

$$\psi(\mathbf{r})=f(\xi)g(\eta)\frac{e^{\pm im\varphi}}{\sqrt{2\pi}} . \tag{33}$$

The principal quantum number is given in terms of the parabolic quantum numbers such that $n=n_1+n_2+m+1$ and is subject to the constraint $A+B=n$ where A and B are the separation constants for the equations in ξ and η, respectively. The upfield coordinate is given by η.

Next, we give a qualitative discussion of the solution of these equations and matrix element calculations. We employ a Rayleigh-Schrödinger perturbation theory solution [32,33] for small-field values. Direct numerical solution is applicable, in principle, for fields of any magnitude, though, in practice, it turns out to be inconvenient for very small-field values because it is difficult to numerically handle the resultant extremely sharp resonances. Consequently, the perturbation and numerical solution techniques are complementary and additionally should serve as consistency checks since they should produce matching results for a suitable intermediate range of fields. For large field values, the resonance nature of the radiator states becomes an important part of their description and perturbation theory is no longer applicable. Therefore for these larger field values, a numerical solution is employed [34].

The presence of the uniform field at the radiator changes the nature of bound atomic states by turning each discrete energy level into a resonance; in other words, there will be a solution for a particular set of quantum numbers that includes a continuum of energy values [35,36]. For a field strength given by ϵ, the states can be characterized uniquely by the quantum numbers m, A, and the energy E. The quantum numbers m and A remain discrete, but E now has a continuous spectrum. For weak-field values, the density of states is sharply peaked about the energy value that corresponds to the discrete state given by the perturbation theory solution to the problem. As the field value increases, however, the density of states broadens and the probability of finding the electron with an energy more widely spaced from the resonance center increases.

Since the values of the energy have a continuous spectrum, we have the normalization condition per unit energy given by

$$\tfrac{1}{4}\int_0^{2\pi}d\varphi\int_0^{\infty}d\xi\int_0^{\infty}d\eta(\xi+\eta)\psi^*_{m_1,A,E}\psi_{m_1',A',E'} =\delta_{m_1,m_1'}\delta_{A,A'}\delta(E-E') . \tag{34}$$

The density of states can be obtained by studying the behavior of the electron probability density near the nucleus [35,36] and can be approximated by the Breit-Wigner parametrization [31]

$$\mathcal{D}^m_{n_1}(E)=\mathcal{D}^m_{n_1}(E_R)\frac{\frac{1}{4}\Gamma^2}{(E-E_R)^2+\frac{1}{4}\Gamma^2} , \tag{35}$$

where E_R corresponds to the energy value at the maximum of the density of states of the resonance and Γ is the full resonance width at half maximum.

Once we have numerically evaluated $f(\xi)$ and $g(\eta)$, we are free to evaluate the matrix elements needed for the line shape. We evaluate the field-dependent matrix element of a real operator $\mathcal{O}$ between two resonance states denoted by subscripts i and j by integrating over the energy range of each resonance. The square of the matrix element for an operator $\mathcal{O}$ can be written as

$$|\mathcal{O}_{i,j}(\epsilon)|^2=\int dE_i\int dE_j|\langle\psi_i(E_i,\epsilon)|\mathcal{O}|\psi_j(E_j,\epsilon)\rangle|^2 . \tag{36}$$

For sufficiently narrow resonances we can approximate this result by

$$\mathcal{O}_{i,j}\approx\left[\frac{\pi\Gamma_i}{2}\right]^{1/2}\left[\frac{\pi\Gamma_j}{2}\right]^{1/2}\langle\psi_i(E_{R,i},\epsilon)|\mathcal{O}|\psi_j(E_{R,j},\epsilon)\rangle , \tag{37}$$

where we have used the value of the eigenfunctions at resonance center $E_{R,j}$. This is a reasonable approximation because the main energy dependence of the wave functions, for narrow resonances, is contained in the normalization factor which is a function of the square root of the density of states. We employ this approximation in all numerical evaluations of atomic matrix elements in this work. Our evaluation of the square of the matrix element allows us to integrate over the density of states to obtain the $\pi\Gamma_i/2$ factors. Since these factors are always positive and real, the sign (and any factors of i) of $\mathcal{O}_{i,j}$ is reliably

given by the evaluation of $\langle\psi_i(E_i,\epsilon)|\mathcal{O}|\psi_j(E_j,\epsilon)\rangle$ at $E_i=E_{R,i}$ and $E_j=E_{R,j}$. As the field ϵ goes to zero, Eq. (36) reduces to the usual zero-field limit.

IV. RESULTS AND DISCUSSION

In the preceding sections we have formulated an extension to the general theory of plasma spectral line broadening and discussed many of the approximations used to arrive at a workable result. This extended theory includes higher-order microfield effects on atomic matrix elements and radiator energy levels. We now present and discuss the results of calculations based on this theory as applied to the L_α and L_β lines of hydrogenic argon.

The presence of these higher-order field effects can be expected to lead to several discernible changes in dense plasma spectral line shapes for the physical conditions we are interested in: $n_e=1\times10^{24}$ to 1×10^{25} cm^{-3} at $kT=800$ eV. In this range, the lowest-order corrections, the ion quadrupole and the quadratic Stark effect, will generally give rise to a blue asymmetry of the spectral line shape; the intensity of the high-energy side of the spectral line will be enhanced over that of the low-energy side. This comes about by the preferential shifting to lower energy of components comprising the manifold of energy levels associated with a principal quantum number n. Energy levels that have been Stark shifted to the low-energy side of the unperturbed upper state of the transition correspond to atomic electrons that are found to have the maximum value of their probability amplitude on the upfield side of the radiator potential well. This corresponds to the side of the origin where the potential barrier has a finite maximum; the other side, the downfield side, corresponds to the potential barrier increasing without bound. The upfield electrons are more easily affected by the field and hence their energy levels are shifted more. This preferential shifting produces a spreading out of intensity on the low-energy side of the line and thus a relative increase in the high-energy side of the line. The addition of the ion quadrupole effect enhances this trend and further adds to the blue asymmetry of the line. The consequences of the field dependence of the wave functions and their resulting matrix elements are more difficult to characterize due to less systematic results on the line shape. Therefore we study this effect only in combination with the other field effects. For sufficiently strong fields, the Stark effect will cause energy levels from adjacent principal quantum number manifolds to overlap. Inclusion of this phenomenon can be important for the accurate representation of line overlap and merging as well as line asymmetry. In this paper, the intensity of all line shapes is multiplied by the ω^4 factor present in Eq. (1) to account for an additional asymmetry [37] and all lines are area normalized to one.

The inclusion of field effects in the case of the L_α line gives rise to a field-dependent fine-structure correction to the radiator Hamiltonian. The field dependence appears in the dipole matrix elements and, because we include the ion quadrupole effect, also in the quadrupole matrix elements. For this transition, at the densities and temperature considered here, the resonance nature of the states is only nominally important and perturbation theory is adequate. The $n=2$ and 3 levels are also well separated in energy for these conditions and do not overlap for relevant field strengths. Consequently, we need not consider this overlap for the L_α line calculation. We have examined the L_α line for $n_e=1\times10^{24}$, 5×10^{24}, and 1×10^{25} cm^{-3} at $kT=800$ eV. As seen in Fig. 2, for the highest density (1×10^{25}), there is little visible difference in the line shape that includes the higher-order field effects as compared to the one using field-independent atomic physics and no ion quadrupole effect. The difference between profiles for the lower densities is even less. We conclude that, for the density range examined in this paper, the plasma microfield is not strong enough for these higher-order effects to become important. If we go much beyond 1×10^{25} cm^{-3}, however, the electron degeneracy will have to be incorporated into the theory to describe the perturbing electrons of the plasma.

The L_β line has its excited state electron in the less tightly bound $n=3$ state. This makes it much more susceptible to the effect of the plasma microfield. To investigate the higher-order effects on this line, we include in our calculations the ion quadrupole effect, field-dependent atomic physics, and the mixing of the levels of principal quantum number $n=3$ and 4.

This last process allows for atomic matrix elements connecting the two principal quantum number manifolds. It also contributes more terms to the sum over intermediate states when evaluating the electron broadening operator $M(\Delta\omega)$. In the field-free atomic physics calculation, this is also possible but the energy levels are more widely separated and their contribution to the sum over intermediate states will be smaller. The decreasing value for large $\Delta\omega$ of the electron broadening many-body function

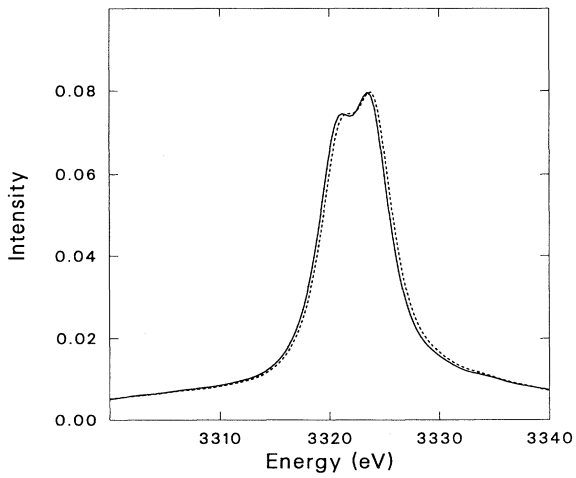

FIG. 2. The L_α line of hydrogenic argon with and without higher-order field effects. The profile with field-independent atomic physics and no ion-quadrupole effect is given by ——. The profile with field-dependent atomic physics and the APEX ion quadrupole effect is given by ------. The density is $n_e=1\times10^{25}$ cm^{-3} and $kT=800$ eV. Both profiles contain fine-structure splitting and are Doppler convoluted. In all energy-intensity plots intensity is in arbitrary units.

$G(\Delta\omega)$ will attenuate each added term if the energy separation between levels is greater than the plasma frequency $\omega_{p,e}$. In the field-dependent atomic physics approach, the zero-order energy levels are perturbed by the Stark effect and can overlap. When this occurs, the $G(\Delta\omega)$ function takes its maximum value for each intermediate state and the total electron broadening term will be larger. In general, the red (blue) levels of a principal quantum number manifold interact most strongly with the red (blue) levels of other manifolds. On the other hand, the red levels of one principal quantum number and the blue levels corresponding to another interact hardly at all [30]. This quasiselection rule causes the electron broadening of the $n=3$ red levels to be most influenced by the red levels of the $n=4$ manifold. Interaction of the blue levels between manifolds is less due to their greater separation in energy. This mechanism contributes a further blue asymmetry to the L_β line by way of a broader red wing caused by this additional electron broadening. These electron broadening effects are illustrated in Fig. 3 where we show the L_β line at $n_e=1\times10^{25}$ cm^{-3} and $kT=800$ eV for the case of full field-dependent atomic physics plus the ion quadrupole effect. This is compared to the same line but with all connections to the $n=4$ levels excluded from the electron broadening of the L_β transition. The mixing between the $n=3$ and 4 manifolds produces a line profile which is approximately 10% broader (width at half intensity) than the line with the restriction on the electron broadening sum. This effect at lower densities has been noted previously by Woltz and Hooper [38] using field-free atomic physics.

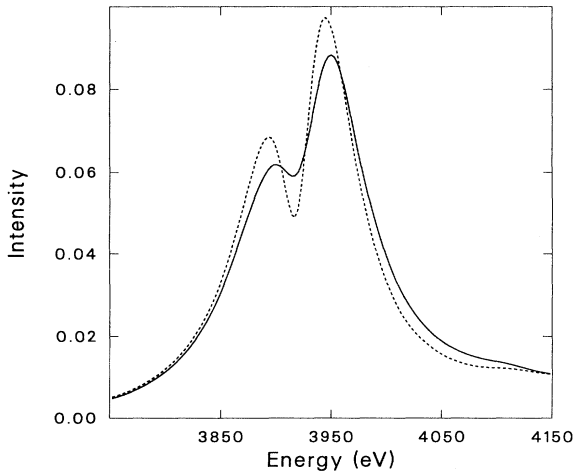

FIG. 3. Comparison of the L_β line of hydrogenic argon with and without electron broadening contributions from the $n=4$ levels. The Stark broadened line shape with field-dependent atomic physics, the ion quadrupole effect, and contributions to electron broadening from dipole matrix elements connecting $n=3$ levels with other $n=3$ levels as well as contributions connecting $n\equiv3$ level with all $n=4$ levels is given by ——. The same line but with all dipole matrix elements connecting the $n=3$ and 4 levels deleted from the sum in Eq. (13), which is used to evaluate the electron broadening operator $M(\Delta\omega)$, is given by (----). Here $n_e=1\times10^{25}$ cm^{-3} and $kT=800$ eV.

The fine-structure splitting for this line is on the order of 2 eV. For $n_e=1\times10^{24}$ cm^{-3}, the overall linewidth is about 40 eV, so we can consequently ignore the much smaller fine-structure splitting. It has been shown [19,39] that this splitting introduces a slight red line asymmetry that will be obscured by the blue symmetry effects as the density increases. The overall shift of the line due to the fine structure is not significant for the line shape and is ignored here.

Before we look at the profiles of the L_β line in detail, we examine energy-level diagrams for the $n=3$ and 4 levels of hydrogenlike argon as a function of the field strength. Figure 4(a) gives the energy levels as a function of the field for the case of field-dependent atomic physics but no ion quadrupole effect. The manifolds for the two levels begins to overlap at values of the unitless field magnitude $\bar{\epsilon}$ slightly greater than one. According to the Inglis-Teller limit [40], this is the point where the two spectral lines merge and become indistinct. This will only occur, however, if both lines are of comparable intensity. In a spectral series the intensity of the lines generally decreases as you go up in the series (as the n value of the upper state increases). As this occurs, we will find that the L_γ line merges with the L_β line but the L_β line itself will still be plainly visible due to its much higher intensity. The Inglis-Teller limit is more accurately applied to lines corresponding to large values of the principal quantum number n, as was noted in the original formulation [40]. For that case the intensities of adjacent lines are similar and their merger will produce an indistinguishable whole.

In Fig. 4(a) we can see the deviation from the linear Stark effect caused by the higher-order corrections to the energy. This is most prominent in the $n=4$ levels. In Fig. 4(b) the Hamiltonian is diagonalized with the ion quadrupole terms added. Now the levels from the two manifolds interact strongly through the field-dependent quadrupole moment matrix elements of the ion quadrupole term. There is a downward shifting of red energy levels of both manifolds and a slight bunching together of the blue levels. When the levels approach each other between these two manifolds, there is strong interaction and level mixing and repulsion are evident. The highest energy (bluest) $n=3$ level experiences a strong avoided crossing with the lowest energy (reddest) $n=4$ level. The energy values in this diagram were calculated from a direct diagonalization of the Hamiltonian [Eq. (27)] for the $n=3$ and 4 levels using field-dependent atomic physics.

The L_β line, without any higher-order field effects or fine structure, is an almost completely symmetric, double-peaked profile. The two levels in the center of the $n=3$ manifold have electric quantum number $q=0$ and are dipole forbidden [see Fig. 4(a)]. This leaves only the outer components which split linearly with the field thus producing the two nearly symmetric peaks. When the ion quadrupole effect is added, the high-energy levels bunch together slightly while the low-energy levels are deflected downward imparting a blue asymmetry to the line. This asymmetry is seen to increase as the density increases in Figs. 5(a)–5(c). In these figures the effect of the

$n=4$ levels is also apparent. The L_γ line is centered at 4133 eV. In Fig. 5(a), at an electron density of $n_e=1\times10^{24}$ cm^{-3} we see a slight increase in the intensity of the blue wing, but as the density increases a broad, flat, blue shoulder develops. At 5×10^{24} cm^{-3}, the L_γ line is flat having merged with the L_β to become the prominent shoulder visible in Fig. 5(b). This illustrates the point made earlier about the Inglis-Teller limit applying only to the less intense member of a pair of merging lines.

Having established the ion quadrupole effect as a source of line asymmetry, we will return to it later to ex-

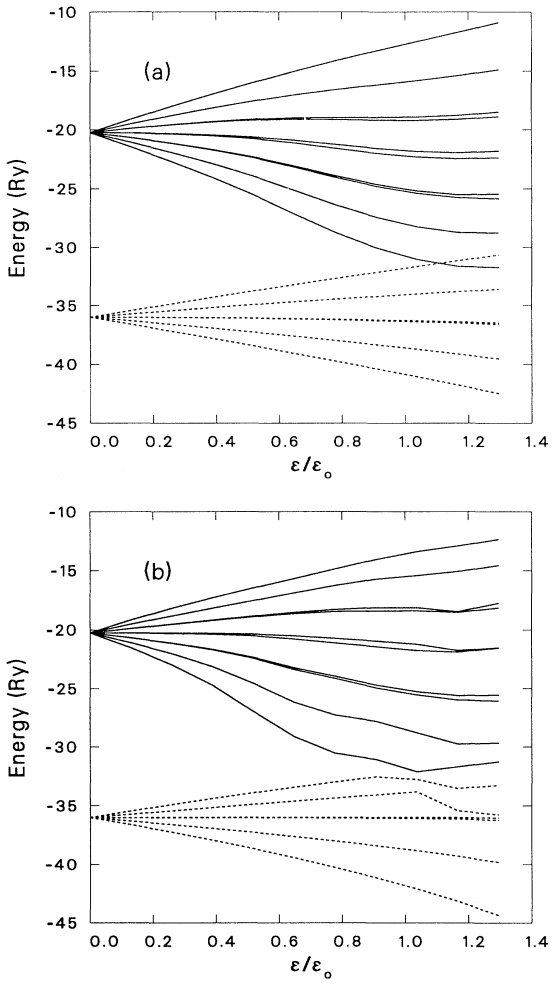

FIG. 4. The energy-level diagram for the $n=3$ and 4 level manifolds as a function of the plasma microfield using field-dependent atomic physics, but no ion quadrupole effect is shown in (a). (b) shows the energy-level diagram for the $n=3$ and 4 level manifolds as a function of the plasma microfield using field-dependent atomic physics and the ion quadrupole effect. The $n=3$ levels are given by ---- and the $n=4$ levels are given by ——. The field is given by the unitless $\tilde{\epsilon}=\epsilon/\epsilon_o$ and the energy is in rydbergs. Note the avoided level crossings introduced by the ion quadrupole perturbations in (4b). The ion quadrupole corrections are calculated in the APEX approximation for $n_e=1\times10^{25}$ cm^{-3} and $kT=800$ eV.

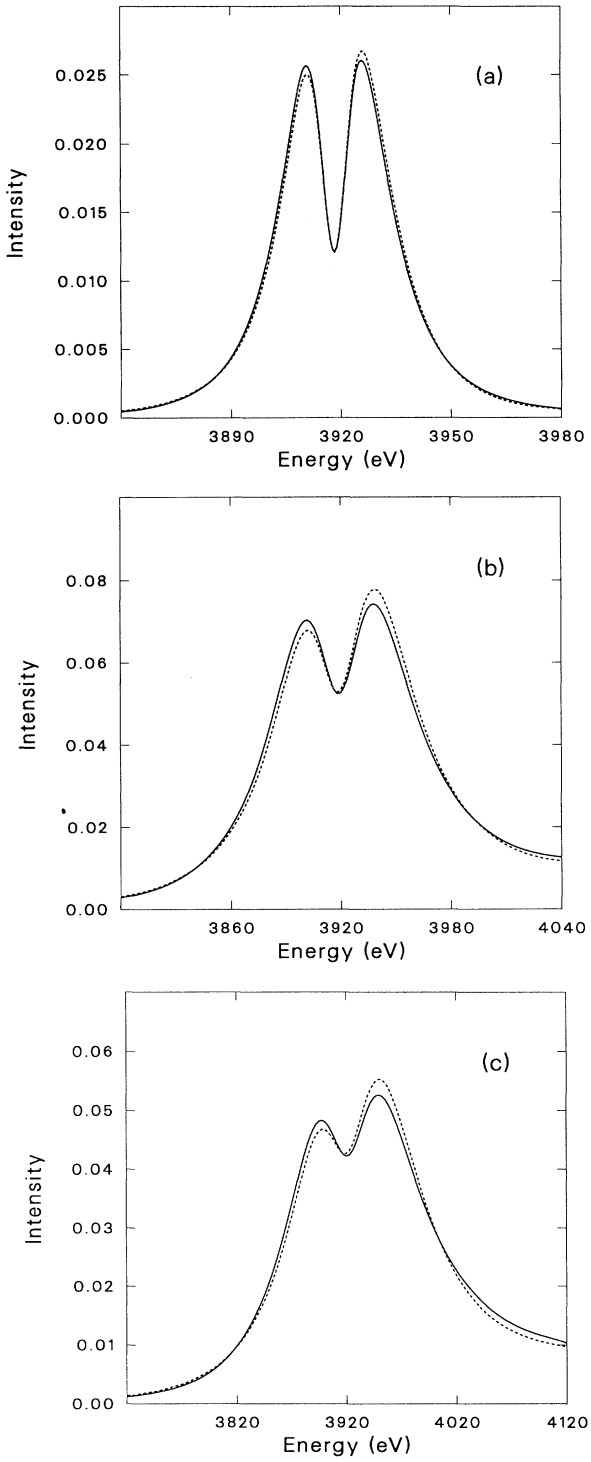

FIG. 5. The L_β line of hydrogenic argon with and without ion quadrupole corrections. The profile with field-independent atomic physics and no ion quadrupole effect is given by ——. The profile with field-independent atomic physics and the APEX ion quadrupole effect is given by ----. (a), (b), and (c) correspond to densities of $n_e=1\times10^{24}$, 5×10^{24}, and 1×10^{25} cm^{-3}, respectively. All three correspond to a temperature of $kT=800$ eV and are Doppler convoluted. Note that energy scales vary from plot to plot.

amine the results of different approaches to its calculation. Now we examine the effect of the field-dependent atomic physics on the L_β line along with the ion quadrupole effect. From the energy-level diagram, we expect the added field dependence to produce further blue asymmetry of the line shape. In Fig. 6(a) we see this beginning for $n_e = 1\times10^{24}$ cm^{-3}. This trend continues in Fig. 6(b) at $n_e = 5\times10^{24}$ cm^{-3}. A check of these additional asymmetries against an approximate quadratic Stark effect calculation [19,39] shows that this asymmetry effect is due primarily to the quadratic correction to the energy. At 1×10^{25} cm^{-3}, however [Fig. 6(c)], the additional asymmetry goes beyond the quadratic correction and can be attributed to higher-order energy shifts and field-dependent changes in the atomic matrix elements. In Figs. 7(a)–7(c) we compare the full field-dependent atomic physics line-shape calculations for a range of densities, with the field-independent atomic physics calculations with the quadratic Stark effect correction to the level energies. Both cases also have the ion quadrupole effect. The quadratic Stark effect correction consists of adding the second-order perturbation theory term from the treatment of an ion in a uniform electric field to the upper state radiator energy levels. This amounts to neglecting all field dependence from the atomic physics except this diagonal energy correction second order in the field. It can be assumed that remaining differences between the two line shapes in the illustrations are due to additional field dependence of the energies, matrix elements, and intensity factors. We conclude that for a temperature of $kT = 800$ eV at the density of $n_e = 5\times10^{24}$ cm^{-3} and below, the field-independent atomic physics plus the approximate quadratic Stark effect correction are good approximations to the full field-dependent results for the L_β line of hydrogenic argon. The resonance widths that are included in these calculations do not add significant width or distortion to the line shape. This is due to the resonance width becoming appreciable only where the electric field is very large, a condition for which the microfield probability function is negligibly small.

We now return to consideration of the three different treatments of the ion quadrupole effect. The NN approximation ignores the many-body effects of other ions in their interaction with each other and with the charged radiator. The APEX approximation is a full many-body treatment that accounts for multiple perturbers as well as the effect of ion-ion correlations. Finally, the IP approximation includes the effect of multiple perturbers but ignores all ion-ion correlations. Both the IP and APEX approximations include the interaction of the perturbing ions with the radiator. As expected from Fig. 1, the line shape for the L_β line employing the NN approximation for the field gradient approaches that using the APEX approximation as the density increases. For $n_e = 1\times10^{25}$ cm^{-3} the two approximations produce line profiles whose maximum intensities differ by no more than 3.2% the NN approximation producing the greater asymmetry. At the lowest density studied here ($n_e = 1\times10^{24}$ cm^{-3}), the intensities differ by no more than 5%. The IP approximation produces line profiles that exhibit less asymmetry

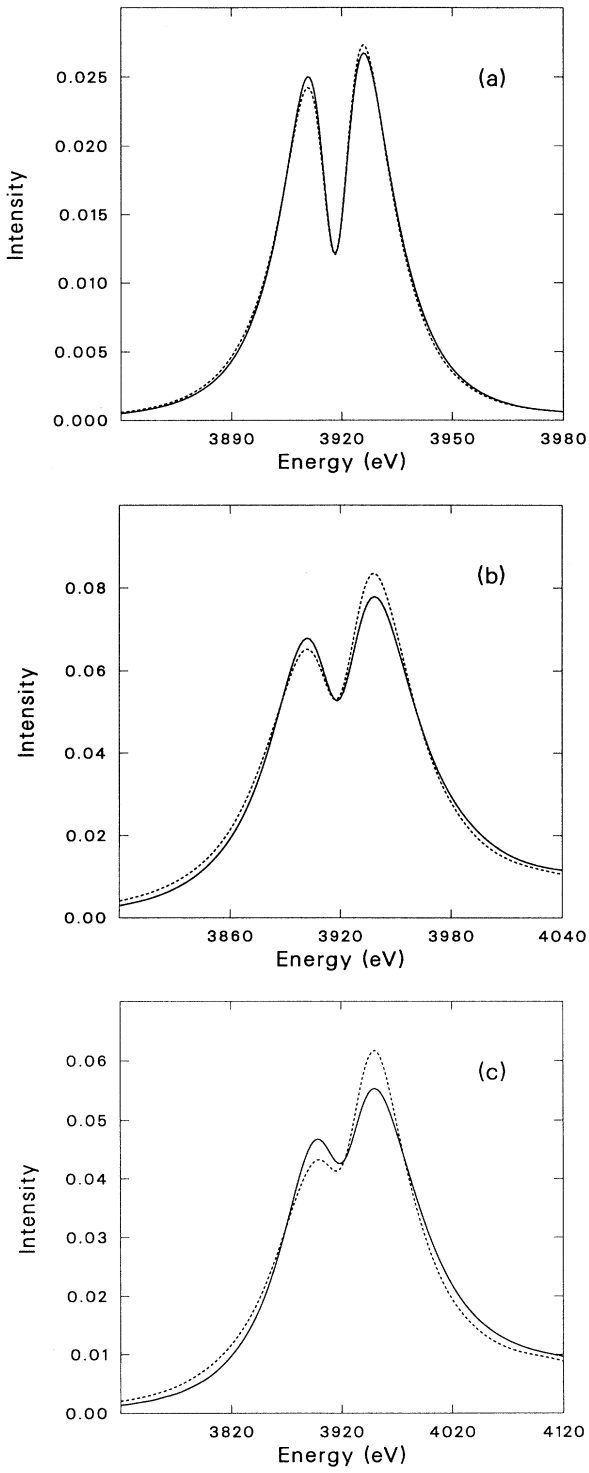

FIG. 6. The L_β line of hydrogenic argon with and without field-dependent atomic physics. The profile with field-independent atomic physics and the APEX ion quadrupole effect is given by ——. The profile with field-dependent atomic physics and the APEX ion quadrupole effect is given by ----. (a), (b), and (c) correspond to densities of $n_e = 1\times10^{24}$, 5×10^{24}, and 1×10^{25} cm^{-3}, respectively. All three correspond to a temperature of $kT = 800$ eV and are Doppler convoluted. Note that energy scales vary from plot to plot.

than either the NN or APEX approximations also as expected from Fig. 1.

This paper has focused on the behavior of additional ion broadening effects on some of the resonance lines of hydrogenic argon. Heliumlike satellite lines, which can appear on the low-energy side of resonance lines, are not considered here, although they have been discussed elsewhere [41]. Additionally, three points regarding uncertainties in the treatment of electron broadening need to be made. First, we have not considered line shifts due to electron collisions in this work. Several theoretical investigations [42,43] have pointed out the possibility of significant line shifts from this source. Since these predicted shifts differ for each line series member, uncertainties could be introduced in our case on the high-energy side of the Lyman-β line for conditions where the Lyman-β and Lyman-γ lines significantly overlap. Second, interference between continuum and line radiation might produce an additional asymmetry effect [44]. This interference has not been included in our treatment, but such processes are currently under investigation. Third, for low-density cases the second-order electron broadening theory is not valid in the line wings and should be replaced by the so-called unified theory [47]. This wing behavior can also be described by Baranger's one-electron theory [45], but is not included here. Attempts to address this are presently under development.

V. CONCLUSIONS

We conclude this investigation by summarizing our findings, pointing out some of their consequences, and suggesting additional steps needed to extend this work to higher densities.

For our range of physical conditions ($n_e = 1\times10^{24}$ to 1×10^{25} cm^{-3} at $kT = 800$ eV) and for the pure argon

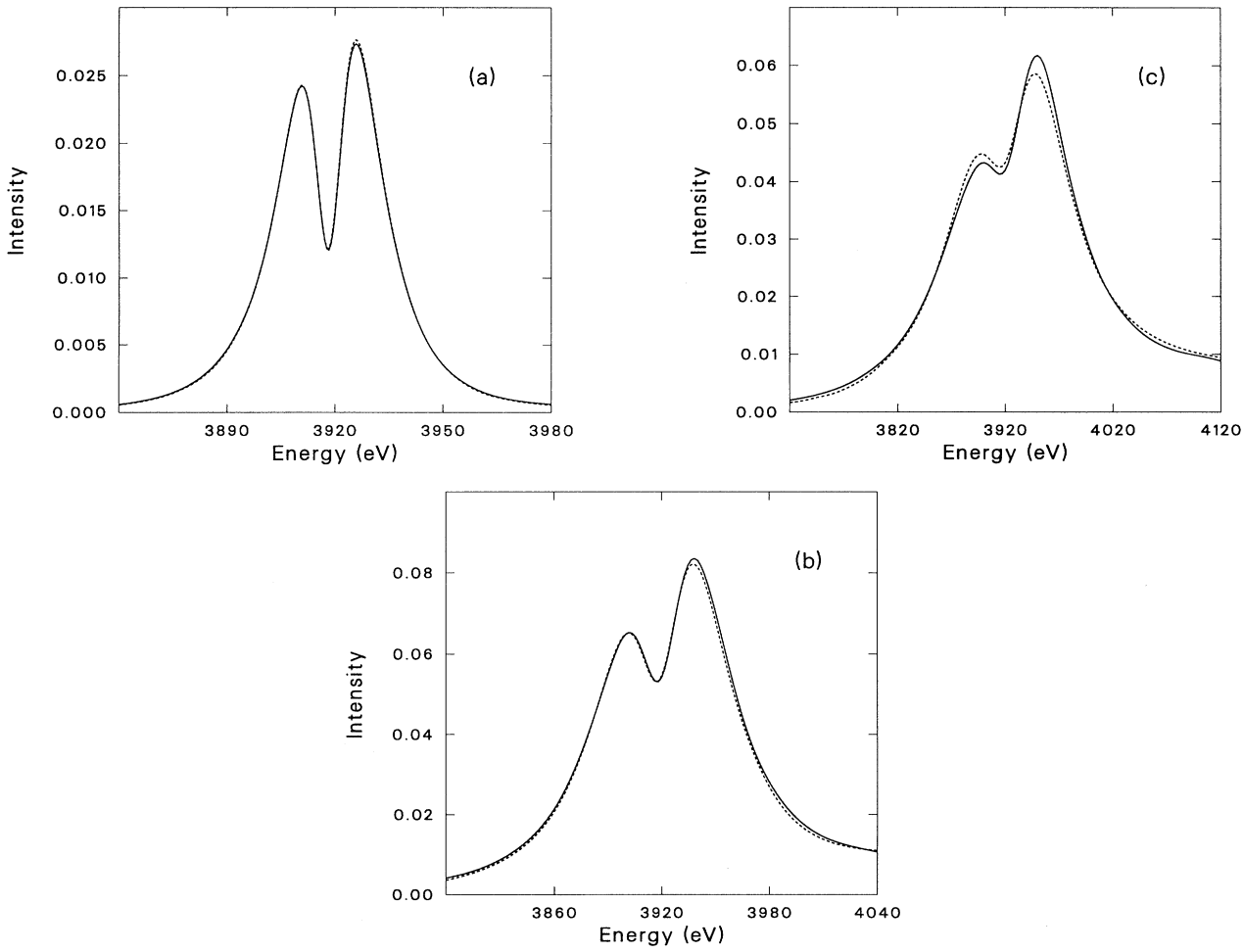

FIG. 7. Comparison of the quadratic Stark effect corrected field-independent atomic physics case to the full field-dependent case for the L_β line of hydrogenic argon. The profile with field-dependent atomic physics and the ion quadrupole effect is given by ——. The profile with field-independent atomic physics, the ion quadrupole effect and the quadratic energy correction is given by ----. (a), (b), and (c) correspond to densities of $n_e = 1\times10^{24}$, 5×10^{24}, and 1×10^{25} cm^{-3}, respectively. All three correspond to a temperature of $kT = 800$ eV and are Doppler convoluted. Note that the quadratic Stark effect correction nearly compensates for the full field-dependent effects except in the highest-density case (c). Note that energy scales vary from plot to plot.

plasma we found that the higher-order field effects begin to become important for the $n=3$ to 1 transition (L_β). The $n=2$ to 1 transition (L_α) showed only very slight perturbations from the linear Stark effect with fine-structure splitting and Doppler broadening. While the fine structure does show a slight field dependence, it produces no significant effect on the line splitting or shape for the L_α line. The L_β line did show many of the additional field effects. The most pronounced was the effect of the field-dependent atomic physics (matrix elements and energy levels that include an exact treatment of the ion dipole term in the radiator Hamiltonian). This field dependence can be well approximated by simply adding the quadratic correction to the level energy for densities of 1×10^{24} to 5×10^{24} cm^{-3}. At $n_e=1\times10^{25}$ cm^{-3}, however, the other field effects on the atomic physics become important and cannot be ignored.

We have also seen that a more accurate treatment of ion-ion correlations in a model of the ion quadrupole effect increases the magnitude of this effect as compared to an IP treatment that does not include these correlations. Additionally, at the very highest densities that we examined, a simple nearest-neighbor model produces a fair approximation to the more accurate results. For densities higher than these the nearest-neighbor approximation may be quite sufficient.

Line merging was also examined. It was demonstrated that it is possible to carry the line-shape calculation to densities beyond the Inglis-Teller merging point. We included the $n=4$ levels in our calculation of the $n=3$ to 1 transition and found that transitions from the $n=4$ level formed a prominent shoulder on the high-energy side of the L_β line.

To carry these line-shape calculations to higher densities for the same temperature range, it will be necessary to include a treatment of degenerate plasma electrons. For densities of $n_e=1\times10^{26}$ cm^{-3} the Fermi energy is of the same order as the thermal energy. When the plasma electrons become degenerate they may not be available for electron collisional broadening [46] and may reduce the electron broadening at high densities.

ACKNOWLEDGMENTS

One of the authors (D.P.K.) would like to thank James Dufty and Carlos Iglesias for helpful discussions and suggestions pertaining to this work. The research reported in this paper was partially supported by U.S. DOE Grants Nos. DE-AS08-88DP10696 and DE-AS08-88DP10780.

APPENDIX

In this appendix we evaluate the constrained average of the field gradient. Initially the constrained average of a general quantity F is developed and specialized to the case of the field gradient at the end. The constrained average $\langle F\rangle_\epsilon$ represents the average, in the presence of the charged radiator, of the quantity F over the ensemble of all possible plasma ion configurations that give the electric-field magnitude ϵ at the origin. This average is given by

$$\langle F\rangle_\epsilon=\frac{\langle F\delta(\epsilon-\mathbf{E})\rangle}{Q(\epsilon)}\ , \tag{A1}$$

where $Q(\epsilon)$ is the plasma microfield function and $\langle\ \rangle$ is the complete perturbing ion subsystem ensemble average. It is possible to relate this constrained average to a functional derivative of the plasma microfield function. This will allow us to evaluate the constrained average in terms of a simplified model for the microfield function $Q(\epsilon)$.

For our purposes we will take F to be an additive function of the ion spatial coordinates,

$$F=\sum_i f(\mathbf{r}_i)=\int d\mathbf{r}\, f(\mathbf{r})n(\mathbf{r})\ , \tag{A2}$$

where

$$n(\mathbf{r})=\sum_i \delta(\mathbf{r}-\mathbf{r}_i)\ . \tag{A3}$$

This leads to

$$\langle F\rangle_\epsilon=\frac{1}{Q(\epsilon)}\int d\mathbf{r}\, f(\mathbf{r})\int\frac{d\lambda}{(2\pi)^3}e^{-i\lambda\cdot\epsilon}\langle n(\mathbf{r})e^{i\lambda\cdot\mathbf{E}}\rangle\ . \tag{A4}$$

We introduce $G(\lambda)$, the generating function of the microfield distribution, where

$$G(\lambda)=\ln\tilde{Q}(\lambda)=\ln\langle e^{i\lambda\cdot\mathbf{E}}\rangle\ . \tag{A5}$$

If we define a function ϕ, such that $\phi=i\lambda\cdot\mathbf{E}(\mathbf{r})$, then $G(\lambda)$ becomes a functional of ϕ, or $G(\lambda)=G[\phi]$. Now we will express $\langle F\rangle_\epsilon$ in the form of a functional derivative. A comparison of Eq. (6) of Ref. [16] and Eq. (A1) of Ref. [25] allows us to establish a connection between the functional derivative $G[\phi]$ and the averaged quantity in Eq. (A4) above to give

$$\langle n(\mathbf{r})e^{i\lambda\cdot\mathbf{E}}\rangle=\langle e^{i\lambda\cdot\mathbf{E}}\rangle\frac{\delta G[\phi]}{\delta(i\lambda\cdot\mathbf{E}(\mathbf{r}))}\ . \tag{A6}$$

Substitution of Eq. (A6) into Eq. (A4) gives us

$$\langle F\rangle_\epsilon=\frac{1}{Q(\epsilon)}\int d\mathbf{r}\, f(\mathbf{r})\int\frac{d\lambda}{(2\pi)^3}e^{-i\lambda\cdot\epsilon}\tilde{Q}(\lambda)\frac{\delta G[\phi]}{\delta(i\lambda\cdot\mathbf{E}(\mathbf{r}))}\ . \tag{A7}$$

This explicitly shows the relationship between the constrained average of F and the functional derivative of the microfield generating function $G(\lambda)$. We are free to use whatever functional model we choose for $\tilde{Q}(\lambda)$.

With the APEX model in Eq. (28) used to evaluate Eq. (A7) we obtain

$$\langle F\rangle_\epsilon=\frac{n_i}{Q(\epsilon)}\int d\mathbf{r}\, f(\mathbf{r})g(r)Q(\epsilon-\mathbf{E}^*(\mathbf{r}))\ , \tag{A8}$$

where it is understood that the microfield distributions $Q(\epsilon)$ are in the APEX approximation. $\mathbf{E}^*(\mathbf{r})$ is the APEX renormalized plasma-ion field given by Eq. (29). For the ion quadrupole effect, the constrained average needed is $\langle E_{zz}\rangle_\epsilon$. In particular, we have

$$F=E_{zz}=\sum_{i=1}^{N}\varepsilon_{zz}(r_i)\ , \tag{A9}$$

where $\varepsilon_{zz}(r_i)$ is the field produced by one of the N perturbing ions. The derivative term is given by

$$\varepsilon_{zz}(r)=Ze\frac{e^{-r/\lambda}}{r^3}\left[1+\frac{r}{\lambda}\right](1-3\cos^2\theta)\ . \tag{A10}$$

The microfield function in the APEX approximation is [15]

$$Q(\epsilon)=\frac{1}{2\pi^2\epsilon}\int_0^\infty dk\ k\sin(k\epsilon)e^{n_i h_1(k)}\ , \tag{A11}$$

with

$$h_1(k)=4\pi\int_0^\infty dr\ r^2 g(r)\frac{E(r)}{E^*(r)}\{j_0[kE^*(r)]-1\}\ , \tag{A12}$$

where $j_0(x)=\sin(x)/x$ is the zero-order spherical Bessel function of the first kind. Using this approximation we can evaluate Eq. (A8) for the case of $F=E_{zz}$ to obtain

$$\langle E_{zz}\rangle_\epsilon=\frac{Zen_i}{2\pi^2 Q(\epsilon)}\times\int_0^\infty dk\ k^2 e^{n_i h_1(k)}\times\int_0^\infty dr\ r^2 g(r)\frac{e^{-r/\lambda}}{r^3}(1-r/\lambda)I_\Omega(r)\ . \tag{A13}$$

The angular integral I_Ω is given by [19]

$$I_\Omega(r)\equiv\int d\Omega(1-3\cos^2\theta)j_0[k|\epsilon-\mathbf{E}^*(r)|]=-8\pi j_2(k\epsilon)j_2[kE^*(r)]\ . \tag{A14}$$

---

*Present address: Theoretical Division, MS-B212, Los Alamos National Laboratory, Los Alamos, NM 87545.

[1] H. R. Griem, *Spectral Line Broadening by Plasmas* (Academic, New York, 1974).

[2] H. R. Griem, Phys. Fluids B **4**, 2346 (1992).

[3] C. F. Hooper, Jr., D. P. Kilcrease, R. C. Mancini, L. A. Woltz, D. K. Bradley, P. A. Jaanimagi, and M. C. Richardson, Phys. Rev. Lett. **63**, 267 (1989).

[4] A. V. Demura and G. V. Sholin, J. Quant. Spectrosc. Radiat. Transfer **15**, 881 (1975).

[5] D. Lambert and M. Louis-Jacquet, J. Phys. (Paris) **46**, 379 (1985).

[6] R. L. Joyce, L. A. Woltz, and C. F. Hooper, Jr., Phys. Rev. A **35**, 2228 (1987).

[7] I. M. Gaisinsky and E. A. Oks, J. Quant. Spectrosc. Radiat. Transfer **41**, 235 (1989).

[8] J. Halenka, J. Quant. Spectrosc. Radiat. Transfer **39**, 347 (1988).

[9] B. d'Etat and H. Nguyen, in *Spectral Line Shapes, Vol. 3,* edited by F. Rostas (de Gruyter, Berlin, 1985).

[10] D. P. Kilcrease, R. C. Mancini, and C. F. Hooper, Jr., in *Radiative Properties of Hot Dense Matter: Sarasota, Florida, 1990,* edited by W. Goldstein, C. Hooper, J. Gauthier, J. Seely, and R. Lee (World Scientific, Singapore, 1991).

[11] D. P. Kilcrease, Ph.D. dissertation, University of Florida, 1991 (unpublished).

[12] R. Stamm, B. Talin, E. L. Pollock, and C. A. Iglesias, Phys. Rev. A **34**, 4144 (1986).

[13] E. W. Smith and C. F. Hooper, Jr., Phys. Rev. **157**, 126 (1967).

[14] L. A. Woltz and C. F. Hooper, Jr., Phys. Rev. A **38**, 4766 (1988).

[15] C. A. Iglesias, H. E. DeWitt, J. L. Lebowitz, D. MacGowan, and W. B. Hubbard, Phys. Rev. A **31**, 1698 (1985).

[16] F. Lado and J. W. Dufty, Phys. Rev. A **36**, 2333 (1987).

[17] E. W. Smith, J. Cooper, W. R. Chappell, and T. Dillon, J. Quant. Spectrosc. Radiat. Transfer **11**, 1547 (1971).

[18] J. D. Jackson, *Classical Electrodynamics* (Wiley, New York, 1975).

[19] R. L. Joyce, Ph.D. dissertation, University of Florida, 1986 (unpublished).

[20] E. W. Smith, C. R. Vidal, and J. Cooper, J. Res. Natl. Bur. Stand. **73A**, 389 (1969).

[21] E. W. Smith, Ph.D. dissertation, University of Florida, 1967) (unpublished).

[22] R. C. Mancini, D. P. Kilcrease, L. A. Woltz, and C. F. Hooper, Jr., Comput. Phys. Commun. **63**, 314 (1990).

[23] L. E. Reichl, *A Modern Course in Statistical Physics* (University of Texas Press, Austin, 1980).

[24] C. A. Iglesias, J. L. Lebowitz, and D. MacGowan, Phys. Rev. A **28**, 1667 (1983).

[25] J. W. Dufty, D. B. Boercker, and C. A. Iglesias, Phys. Rev. A **31**, 1681 (1985).

[26] J. W. Dufty, in *Strongly Coupled Plasma Physics,* edited by F. Rogers and H. Dewitt (Plenum, New York, 1987).

[27] F. J. Rogers, Phys. Rev. A **29**, 868 (1984).

[28] J. Dufty and L. Zogaib, Phys. Rev. A **44**, 2612 (1991).

[29] M. Baranger and B. Mozer, Phys. Rev. **115**, 521 (1959).

[30] H. A. Bethe and E. E. Salpeter, *Quantum Mechanics of One- and Two-Electron Atoms* (Plenum, New York, 1977).

[31] L. D. Landau and E. M. Lifshitz, *Quantum Mechanics: Non-Relativistic Theory,* 2nd ed. (Pergamon, Oxford, 1965).

[32] N. Hoe, E. Banerjea, H. W. Drawin, and L. Herman, J. Quant. Spectrosc. Radiat. Transfer **5**, 835 (1965).

[33] N. Hoe, B. D'Etat, J. Grumberg, M. Caby, E. Laboucher, and G. Coulaud, Phys. Rev. A **25**, 891 (1982).

[34] R. Mancini and C. F. Hooper, Jr., Rev. Sci. Instrum. **59**, 1512 (1988).

[35] E. Luc-Koenig and A. Bachelier, J. Phys. B **13**, 1743 (1980).

[36] E. Luc-Koenig and A. Bachelier, J. Phys. B **13**, 1769 (1980).

[37] H. R. Griem, Z. Phys. **137**, 280 (1954).

[38] L. A. Woltz and C. F. Hooper, Jr., Phys. Rev. A **30**, 468 (1984).

[39] L. A. Woltz and C. F. Hooper, Jr., in *Radiative Properties of Hot Dense Matter: Sarasota, Florida, 1983,* edited by J. Davis, C. Hooper, R. Lee, A. Merts, and B. Rozsnyai (World Scientific, Singapore, 1985).

[40] D. R. Inglis and E. Teller, Astrophys. J. **90**, 439 (1939).

[41] L. A. Woltz, V. L. Jacobs, C. F. Hooper, Jr., and R. C. Mancini, Phys. Rev. A **44**, 1281 (1991).

[42] H. R. Griem, M. Blaha, and P. C. Keeple, Phys. Rev. A **41**, 5600 (1990).
[43] E. Koenig, P. Malnoult, and H. Nguyen, Phys. Rev. A **38**, 2089 (1988).
[44] D. D. Burgess, Phys. Rev. **176**, 150 (1968).
[45] M. Baranger, in *Atomic and Molecular Processes,* edited by D. R. Bates (Academic, New York, 1962).
[46] D. Boercker, Ph.D. dissertation, University of Florida, 1978 (unpublished).
[47] E. W. Smith, J. Cooper, and C. R. Vidal, Phys. Rev. **185**, 140 (1969).